DEFENSE TECHNICAL INFORMATION CENTER

Information for the Defense Community

DTIC® has determined on 28/12/2009 that this Technical Document has the Distribution Statement checked below. The current distribution for this document can be found in the DTIC® Technical Report Database.

☒ **DISTRIBUTION STATEMENT A.** Approved for public release; distribution is unlimited.

☐ **© COPYRIGHTED**; U.S. Government or Federal Rights License. All other rights and uses except those permitted by copyright law are reserved by the copyright owner.

☐ **DISTRIBUTION STATEMENT B.** Distribution authorized to U.S. Government agencies only (fill in reason) (date of determination). Other requests for this document shall be referred to (insert controlling DoD office)

☐ **DISTRIBUTION STATEMENT C.** Distribution authorized to U.S. Government Agencies and their contractors (fill in reason) (date of determination). Other requests for this document shall be referred to (insert controlling DoD office)

☐ **DISTRIBUTION STATEMENT D.** Distribution authorized to the Department of Defense and U.S. DoD contractors only (fill in reason) (date of determination). Other requests shall be referred to (insert controlling DoD office).

☐ **DISTRIBUTION STATEMENT E.** Distribution authorized to DoD Components only (fill in reason) (date of determination). Other requests shall be referred to (insert controlling DoD office).

☐ **DISTRIBUTION STATEMENT F.** Further dissemination only as directed by (inserting controlling DoD office) (date of determination) or higher DoD authority.

Distribution Statement F is also used when a document does not contain a distribution statement and no distribution statement can be determined.

☐ **DISTRIBUTION STATEMENT X.** Distribution authorized to U.S. Government Agencies and private individuals or enterprises eligible to obtain export-controlled technical data in accordance with DoDD 5230.25; (date of determination). DoD Controlling Office is (insert controlling DoD office).

JOURNAL OF GEOPHYSICAL RESEARCH, VOL. 113, D10208, doi:10.1029/2007JD009065, 2008

A system for operational aerosol optical depth data assimilation over global oceans

Jianglong Zhang,[1,2] Jeffrey S. Reid,[1] Douglas L. Westphal,[1] Nancy L. Baker,[1] and Edward J. Hyer[1]

Received 12 June 2007; revised 8 October 2007; accepted 21 February 2008; published 31 May 2008.

[1] In this study, we present an aerosol data assimilation system destined for operational use at the Fleet Numerical Meteorological and Oceanographic Center (FNMOC). The system is an aerosol physics version of the Naval Research Laboratory (NRL) Atmospheric Variational Data Assimilation System (NAVDAS) that is already operational. The purpose of this new system, NAVDAS-Aerosol Optical Depth (NAVDAS-AOD) is to improve the NRL Aerosol Analysis and Prediction System (NAAPS)'s forecasting capability by assimilating observational data sources with NAAPS forecast fields. This will allow for not only improved aerosol forecasting but also for dramatically enhanced global scale research capabilities for the study of aerosol-meteorology interaction. NAVDAS-AOD assimilates a newly developed over-water Moderate-Resolution Imaging Spectroradiometers (MODIS) level 3 aerosol product with NAAPS. This paper is the second in a series which describes NRL's program to realistically monitor global aerosol distributions. Here we explain the reasons and procedures for constructing the over-water level 3 MODIS aerosol product, describe the theoretical basis for NAVDAS-AOD, and provide a thorough statistical error analysis for both the MODIS observations and the NAAPS model background fields that are critical to aerosol data assimilation. Using 5 months of analysis, our study shows that by carefully screening over-water satellite observations to ensure only the best quality data are used in the aerosol assimilation process, the NAVDAS-AOD can significantly improve the NAAPS global aerosol optical depth analysis as well as improve the aerosol forecast skill.

Citation: Zhang, J., J. S. Reid, D. L. Westphal, N. L. Baker, and E. J. Hyer (2008), A system for operational aerosol optical depth data assimilation over global oceans, *J. Geophys. Res.*, *113*, D10208, doi:10.1029/2007JD009065.

1. Introduction

[2] The relatively recent use of multichannel, multiangle observations from the Moderate-Resolution Imaging Spectroradiometers (MODIS) and Multiangle Imaging Spectroradiometer (MISR) instruments has dramatically improved spatial and spectral observations of aerosol optical depth (AOD). Recent developments also include algorithmic advancements (including more realistic optical models), better aerosol detection, and improvements in cloud screening capabilities [e.g., *Kaufman et al.*, 2002]. The accuracy of satellite aerosol optical depth retrievals and screening has improved to a point where numerical aerosol forecasting can also benefit from satellite observations through the data assimilation process [*Zhang and Reid*, 2006].

[3] The idea of assimilating satellite observations into numerical models is now commonplace. Some successful applications include assimilation of a satellite wind product [*Tomassini et al.*, 1999], satellite-retrieved surface temperature [*Dabberdt and Schlatter*, 1996], and direct assimilation of satellite radiances [*McNally and Vesperini*, 1996]. However, only a few attempts have been made to assimilate satellite aerosol products into numerical models using an optimal interpolation (OI) technique, mainly through retrospective studies or limited regional studies [e.g., *Yu et al.*, 2004; *Collins et al.*, 2001, *Rasch et al.*, 2001] and most recently through radiance assimilation [*Weaver et al.*, 2007]. No attempt has ever been made to assimilate satellite aerosol optical depth products in a truly operational fashion globally. This is largely because observations and numerical models have only recently improved to the point where serious attempts at satellite aerosol assimilation can begin. Successful data assimilation requires that the observations and the forecast model are sufficiently accurate and have roughly similar quality. Moreover, operational aerosol data assimilation requires processed data to be accessible within 12 h of the satellite overpass time.

[4] Recently, *Weaver et al.* [2007] demonstrated the concept of directly assimilating MODIS radiances in into the Goddard Chemistry and Aerosol Radiation Transport model (GOCART) using an offline assimilation system. However, given the operational constraints of a global

[1]Marine Meteorology Division, Naval Research Laboratory, Monterey, California, USA.
[2]Now at Department of Atmospheric Sciences, University of North Dakota, Grand Forks, North Dakota, USA.

0148-0227/08/2007JD009065$09.00

forecasting system, here we choose to use the conventional aerosol products that are widely accepted through the community. We optimistically assume that the algorithms are accurate and that instrument-specific biases have been eliminated by the developers or at least accounted for in the reported error statistics and described in publications. By using aerosol products such as operational MODIS aerosol product, we are taking advantage of years of work by many different groups to develop and validate these products [e.g., *Remer et al.*, 2005; *Hsu et al.*, 2006; *Husar et al.*, 1997; *Kahn et al.*, 2005]. An aerosol assimilation system that uses aerosol optical depth (AOD) instead of radiances can be easily expanded to include observations from other existing or future sensors; again, provided the error statistics are known. Validation of the AOD observations, forecasts, and analyses is more easily performed since AOD is a commonly measured quantity (e.g., Aerosol Robotic Network (AERONET) global network of Sun photometers [*Holben et al.*, 1998]). Last, the success of radiance assimilation depends on the accuracy of forecasted temperature and moisture fields. Assimilation of AOD avoids this immediate dependency.

[5] In any data assimilation process, high data quality is required, and biases and noises in the observational data must be carefully examined. Large uncertainties exist in aerosol products, especially for over land retrievals where bright heterogeneous surface characteristics pose a challenging problem [*Levy et al.*, 2007]. Studies have also shown that even with the relatively accurate aerosol retrievals over oceans, extra quality assurance steps need to be taken before implementation of the aerosol product into models [*Zhang and Reid*, 2006]. A careful data screening process is needed to remove noisy data, correct biases, and ensure only the best quality data are used in an aerosol data assimilation scheme.

[6] Currently, there are three aerosol products that are created in a near real time mode and could be used in the data assimilation process: MODIS, AVHRR, and TOMS/OMI. Among the three products, we chose the Aqua and Terra MODIS aerosol products due to their fine spectral, spatial, and temporal resolutions. Comparing with previous sensors such as AVHRR, the MODIS products have demonstrated superior performance in both cloud and aerosol detections [*Remer et al.*, 2005; *Zhang and Reid*, 2006].

[7] This paper is the second in a series which outlines advances in the Naval Research Laboratory's (NRL's) global aerosol data assimilation and modeling program. The first provided a thorough analysis of correction factors for MODIS over-ocean aerosol optical depth products for use in data assimilation [*Zhang and Reid*, 2006]. Here we present one of the world's first aerosol data assimilation systems suitable for operation use that assimilates the quality controlled (QC) and quality assured (QA) MODIS over-water aerosol product described in that previous paper with NAAPS forecast fields. For the data assimilation package, we adopted and modified the NRL Atmospheric Variational Data Assimilation System (NAVDAS), which has been used operationally for assimilation of conventional and satellite-based observations [*Baker et al.*, 2005]. In contrast with previous aerosol assimilation efforts [*Collins et al.*, 2001; *Yu et al.*, 2004], we use a 2-D variational approach. In comparison to the OI technique, the 2-D, 3-D, and 4-D variational techniques are more suitable for operational use since local data selection is unnecessary and a more powerful statistical error analysis can be applied.

[8] In this manuscript, we present an outline of the NAVDAS Aerosol Optical Depth package (NAVDAS-AOD). Data screening processes for the operational MODIS over-water aerosol product are briefly summarized. Focus points include a study of the error covariance matrix of the NAAPS model (background) field, an evaluation of the performance of 5 months of MODIS aerosol assimilation using NAVDAS-AOD, and the impact on the first 48 h of NAAPS aerosol forecasts.

2. Satellite Data

[9] In NAVDAS-AOD, Terra (MOD04) and Aqua (MYD04) MODIS level II aerosol products are collected from the NOAA NESDIS Near Real Time Processing Effort (NRTPE) which is produced with a latency of 3 h or less in most cases. NRTPE is a joint effort from NASA, NOAA, Air Force Weather Agency, the Naval Research Laboratory, and the Naval Oceanographic Office. With its reliable data link and short data latency, NRTPE has proven to be one of the best data sources for operational near-real time data. For the study presented here, NAVDAS-AOD is tested with 5 months of data collected from January to May 2006.

[10] MODIS has a total of 36 spectral channels ranging from near-ultraviolet to infrared. Over global oceans, an optimal minimization technique is applied to six spectral channels (ranging from 0.55 to 1.2 μm) for retrieving aerosol optical depth (τ) and aerosol size parameter [*Remer et al.*, 2005]. Although MODIS can provide aerosol retrievals at multiple channels, the aerosol τ in this paper refers to τ at 0.55 μm. Although only one channel information is used in this study, the utilization of the spectral signatures from multiple channels is important and is subject to future studies. *Remer et al.* [2005] gave an overall accuracy for over-water aerosol optical depth of $0.03 \pm 0.05\ \tau$. However, *Zhang and Reid* [2006] showed that systematic biases exist in MODIS over-water aerosol retrievals. These are related to cloud fraction and contamination, aerosol type, and near-surface wind speed impacting the lower boundary condition. Empirical corrections were proposed and data screening strategies were applied to remove outliers. In this study, we adopted the empirical corrections and data screening processes described by *Zhang and Reid* [2006] where a total of 40% data were lost but 70% of the significant outliers were removed. This strict QA procedure is necessary to remove these outliers that would adversely impact the model and propagate through the system, particularly in the middle- to high-latitude oceans.

[11] After the empirical corrections and data screening procedures, MODIS τ data is binned into $1^\circ \times 1^\circ$ latitude/longitude grids to form a 6 hourly, data assimilation quality, Level 3 product (e.g., at NAAPS time of t = 6 h, we used both Terra and Aqua MODIS data from t = 3 h to t = 9 h). In this step, we further exclude data entries with MODIS cloud fraction larger than 30%. We also add an additional QC procedure by removing bins that are isolated from other continuous aerosol features and bins with less than five valid data entries. The additional QC procedures are included to minimize erroneous aerosol features in MODIS

aerosol product that are introduced by cloud artifacts [*Zhang et al.*, 2005; *Zhang and Reid*, 2006].

[12] The QA and QC procedures described in this paper, however, are different from traditional data assimilation approaches where noises in observations are removed based on innovation (difference in observations and forecasts) checks [e.g., *Dee et al.*, 2001]. We argue that external QA and QC checks are necessary for aerosol data assimilation because of the following reasons:

[13] 1. Innovation checks could not flag cases when both observations (O) and forecasts (F) have large biases, yet O minus F values are small.

[14] 2. The efficiency of observations noise removal could be sensitive to arbitrary thresholds used in the innovation checks.

[15] 3. Large innovation values could be valid in cases newly formed aerosol plumes with significant AOD values which models fail to predict. Examples of such cases are biomass burning events with fire hot spots under cloud covers. Aerosol forecasting models such as NAAPS rely on satellite detected hot spots to define their emission sources for biomass burning aerosols. Missing satellite-detected hot spots will cause models to miss a possible significant biomass burning episode. However, with bias correction, it is possible to include such cases, as will be discussed in later part of the text [*Dee and da Silva*, 1999].

[16] 4. By performing QA with this method, we can generate a data assimilation quality level 3 product that is applicable to any model, not just NAAPS/NAVDAS-AOD.

3. Description of the NAAPS Model

[17] With its transition to the Fleet Numerical Meteorology and Oceanography Center (FNMOC) in October of 2006, NAAPS is the U.S. Navy's (and the world's first) truly operational global aerosol forecast model. NAAPS produces 6-d forecasts of SO_2, sulfate, dust, biomass burning smoke and sea salt mass concentration with $1^\circ \times 1^\circ$ resolution on 30 vertical levels [*Witek et al.*, 2007].

[18] The NAAPS global model is a modified form of a hemispheric model of sulfate aerosols developed by *Christensen* [1997]. NAAPS is an offline model that utilizes the meteorological analysis and forecast fields from the Navy Operational Global Analysis and Prediction System (NOGAPS) [*Hogan and Rosmond*, 1991; *Hogan and Brody*, 1993]. Dynamical fields from NOGAPS are remapped to 1° resolution from the 0.5° native NOGAPS resolution. Twice daily, the NOGAPS weather forecast model provides dynamical fields to NAAPS at 6-h intervals for the 6-d forecast period. Transport is calculated using a 3-D semi-Lagrangian scheme [*Staniforth and Cote*, 1991] with departure points calculated using the method of *Ritchie* [1987].

[19] Modifications have been made to the interpolation of wind and concentration fields across the poles, and the interpolation method was changed from a third-order Lagrangian to fifth-order Lagrangian. Horizontal and vertical diffusion are calculated with a finite element scheme. The vertical diffusion coefficient parameterization K_z is based on the Monin-Obukhov similarity theory for the surface layer using the input NOGAPS data. The K_z profile is extended to the whole boundary layer by using a simple extrapolation height of the mixing layer. The horizontal diffusion coefficient is set to a nominal value of $6 \times 10^4\ m^2\ s^{-1}$. The condensation/precipitation scheme is derived from the NOGAPS atmospheric model and is further described in the work of *Hogan and Rosmond* [1991]. These cloud profiles are used to calculate the wet removal and reaction rates of the various species. The dry deposition velocity is based on the resistance method [*Voldner et al.*, 1986; *Walcek et al.*, 1986; *Slinn and Slinn*, 1980], where the deposition velocity depends on the turbulence of surface layer and surface type (ocean, grassland, etc.).

[20] Aerosol source functions come from a variety of static and dynamical algorithms. Sulfur dioxide emission is based on the GEIA inventory, version 1A, for the year 1985 with a seasonal variation and two-level vertical distribution [*Benkovitz et al.*, 1996]. Natural emissions of DMS are immediately converted to 95% sulfur dioxide and 5% sulfate. The gas-phase chemistry is described by a simple linear reaction rate, which depends on the time of year and latitude [*Christensen*, 1997]. Dust emission occurs whenever the NOGAPS friction velocity exceeds a threshold value and the surface moisture is less than 0.3. The threshold friction velocity is set to infinity except in known dust-emission areas where it is 60 cm s^{-1} [*Westphal et al.*, 1988]. These areas are currently defined as areas covered by the erodible land-use types used in the USGS Land Cover Characteristics Database with modification guided by an analysis of TOMS aerosol index. Smoke emissions are based on the Fire Locating and Modeling of Burning Emissions (FLAMBE) source functions based on near-real time geostationary and MODIS fire products [*Reid et al.*, 2004].

4. Overview of the Aerosol Data Assimilation Package

[21] NAVDAS-AOD is founded on the 3-D variational analysis option of the NRL Atmospheric Variational Data Assimilation System (NAVDAS) [*Daley and Barker*, 2001]. NAVDAS is an operational three-dimensional variational data assimilation suite for generating atmospheric state estimates to satisfy a variety of U.S. Navy needs. NAVDAS is formulated in observation space. The preconditioned conjugate gradient method [*Daley and Barker*, 2001] is used to minimize the cost function, which can be understood as the process to minimize the analysis error variance in linear cases. The number of iterations required to reach convergence is minimized through the use of dual block diagonal preconditioners with Choleski decomposition. Forward operators are formulated and used for the direct assimilation of Advanced Television Infrared Observation Satellite Operational Vertical Sounder (ATOVS) radiances and SSM/I wind speeds and total precipitable water. NAVDAS also contains a comprehensive diagnostic suite, including complete observation traceability, Web-based observation monitoring, chi-square monitoring of innovations, the adjoint of the assimilation system, and analysis error variance estimation.

[22] The traditional objective in data assimilation is to create a new analysis field by correcting the background field (i.e., the current model stage) using observations, and then use the new analysis field as an initial condition for future model runs. In the case of the assimilation of a two-

dimensional variable such as optical depth (τ), we degraded NAVDAS from 3-D to 2-D variational approach with three steps:

[23] 1. Preprocessing: a process to convert NAAPS mass concentration to aerosol optical depth:

$$\tau_{b\lambda} = H_{m\_\tau}(C_m) + \varepsilon_{b\lambda} \quad (1)$$

where, $\tau_{b\lambda}$ is the background (prior forecast) aerosol optical depth vector, C_m is the NAAPS mass concentration, and H_{m_τ} is the forward operator that represents the transformations from NAAPS mass concentration to optical depth (see section 4.1 for detail discussions of H_{m_τ}). $\varepsilon_{b\lambda}$ is the error in $\tau_{b\lambda}$ introduced by the H_{m_τ} operator.

[24] 2. Two-D variational assimilation of the optical depth field

$$\tau_{a\lambda} = \tau_{b\lambda} + P_b H^T \left[HP_b H^T + R\right]^{-1} [\tau_{a\lambda} - H(\tau_{b\lambda})], \quad (2)$$

where $\tau_{a\lambda}$ is the analysis optical depth vectors, $\tau_{o\lambda}$ is the observation optical depth vector, and H is the observation operator that represents any necessary spatial and temporal interpolations from background to the observational space. P_b and R are the background error covariance and the observation error covariance matrices, respectively.

[25] The analysis field ($\tau_{a\lambda}$) can be regarded as background ($\tau_{b\lambda}$) plus a correction term ($\hat{\tau}_\lambda$, also $P_b H^T [HP_b H^T + R]^{-1} [\tau_{o\lambda} - H(\tau_{b\lambda})]$), where the correction term is the difference between the observation and background vectors weighted by the ratio of background error covariance matrix to total error covariance matrix in the observational space (with H operator).

[26] 3. Postprocess: a process to convert $\tau_{a\lambda}$ to NAAPS mass concentration:

$$C_m = H_{\tau\_m}(\tau_{a\lambda}) + \varepsilon_m \quad (3)$$

where H_{τ_m} is the backward operator that represents the transformations from optical depth to NAAPS mass concentration. ε_m is the error in C_m introduced by the H_{τ_m} operator. Details of the H_{τ_m} operator will be discussed in section 4.3. Both ε_m and $\varepsilon_{b\lambda}$ could be transformed as part of the bias term of $\tau_{b\lambda}$, which is assumed to be zero for this study. The background bias correction will be discussed further in the later part of this paper.

[27] The NAAPS prognostic variable is the 3-D aerosol mass concentration. In this study, we reduced the problem to a 2-D variational assimilation approach simply because the operational MODIS aerosol product only provides column integrated aerosol optical properties (2-D). With the use of 3-D observations of aerosol optical properties from CALIPSO or through the height information available from some gas retrievals, it is feasible in some circumstances to extend equation (2) to a 3-D variational approach in future studies.

[28] A flowchart of the NAVDAS-AOD process is shown in Figure 1. Four major steps are included: (1) Convert NAAPS mass concentration to $\tau_{b\lambda}$ (3-D to 2-D conversion); (2) run NAVDAS 2-D var to create a new analysis field $\tau_{a\lambda}$ from $\tau_{b\lambda}$ and $\tau_{o\lambda}$; (3) improve the NAAPS mass concentration field using $\tau_{a\lambda}$ (2-D to 3-D conversion); and (4) use the new mass concentration field as an initial condition for the next 6-h NAAPS run.

4.1. NAAPS Aerosol Mass to Optical Depth Transfer Function (H_{τ_m} operator)

[29] In the first step, τ_b values are estimated from NAAPS 3-D mass concentration (g/m^3) using a bulk model:

$$\tau_{b\lambda} = \sum_i \alpha_{ei}(\lambda)^* C_{mi}^* f_{ei}(RH, \lambda) \quad (4)$$

where for each species i and wavelength λ, $\tau_{b\lambda}$ is the wavelength dependent background aerosol optical depth, $\alpha_e(\lambda)$ is the wavelength dependent mass extinction efficiency (m^2 g^{-1}), and C_m is the acrosol particle mass concentration (g m^{-3}) and f_e(RH, λ) is the aerosol hydroscopic growth factor for extinction. For this first generation model, mass extinction cross sections (as a function of wavelength) for dry dust, sulfate, and sea salt are

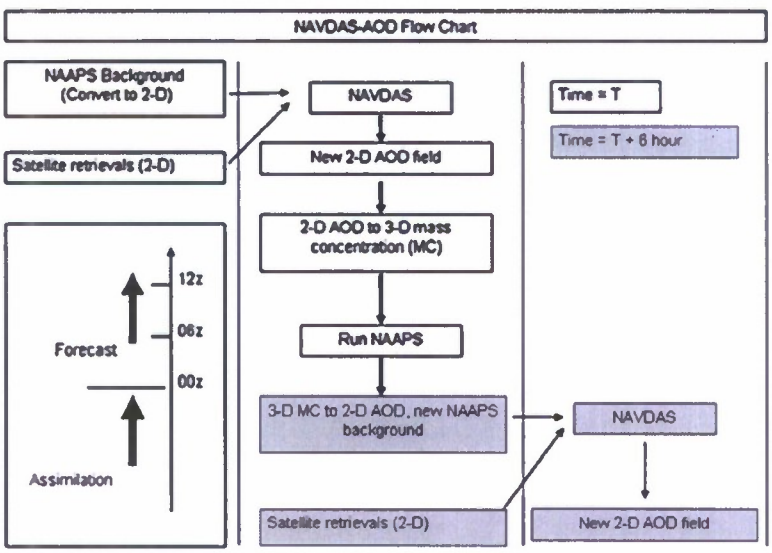

Figure 1. Flowchart of the NAVDAS-AOD.

obtained from Optical Properties of Aerosols and Clouds (OPAC) [*Hess et al.*, 1998]. The parameters used in this section of study may be updated when new observational parameters are available. Smoke properties are derived from *Reid et al.* [2005]. The aerosol hygroscopic growth factor for aerosol absorption coefficient and dust scattering coefficient are assumed to be zero. The aerosol hygroscopic growth factor for sulfate and smoke scattering coefficients are estimated based on *Hanel* [1976] and *Reid et al.* [2005], respectively. The aerosol hygroscopic growth factor for sea salt extinction coefficient is estimated from *Hegg et al.* [2002] and *Ming and Russell* [2001].

[30] It is well understood that that aerosol physical and optical properties vary regionally and are highly event based. Therefore, using generalized aerosol optical properties could introduce uncertainties ($\varepsilon_{b\lambda}$) in the estimated τ_b values. But for the purpose of radiation studies, aerosol optical depth and extinction are the variables of interest. The use of a bulk model in this way, while at time unphysical with respect to aerosol mass, ensures consistency in the atmospheric radiation fields. Indeed, the area of mass extinction efficiencies and extinction to mass transfer function is an area of intensive research in the community.

4.2. Creation of the Optical Depth Analysis Field

[31] In the second step, both observation ($\tau_{o\lambda}$, 2-D) and the background ($\tau_{b\lambda}$, 2-D) vectors developed in step 1 are interpolated to the observational domain, and a new analysis vector ($\tau_{b\lambda} + \hat{\tau}_\lambda$, 2-D) is created by correcting background vector from observations as showed in equation (2). To estimate $\hat{\tau}_\lambda$, both background and observational error covariance matrices are required. In this study, background and observational error covariance are defined as spatial error covariance and are assumed to be independent from meteorological parameters such as wind speed. The nature of the observational and background error variance and error covariance fields will be discussed in detail in section 5.

4.3. Reciprocal Analysis Optical Depth to Mass Concentration Transfer Function (H_{τ_m} Operator)

[32] The third step in the optical depth data assimilation process is to apply $\hat{\tau}_\lambda$ to update the NAAPS mass concentration field. While it is relatively straightforward to go from 3-D to 2-D as in section 4.1, without additional information the converse is ill-posed. To correct the background to the analysis field, where do we add or subtract aerosol particle mass (in vertical and compositional dimensions)? Further, how do we know the differences between errors in mass and hygroscopicity (either through the parameter or the NOGAPS RH field itself)?

[33] Our current solution is to keep the transfer function straightforward and traceable. If $\hat{\tau}_\lambda$ is less than zero, which indicates $\tau_{b\lambda}$ is higher than $\tau_{a\lambda}$, the ratio of $(\tau_{b\lambda} + \hat{\tau}_\lambda)/\tau_{b\lambda}$ is used to reduce the amplitude of mass concentration vertical profile of a given air column; i.e., the concentration in each vertical level is reduced by the same fractional amount, and same for each aerosol composition. If $\hat{\tau}_\lambda = 0$, $\tau_{a\lambda}$ equals to $\tau_{b\lambda}$, and no change is made to the air column. If $\hat{\tau}_\lambda > 0$, $\tau_{b\lambda}$ is lower than $\tau_{a\lambda}$, then the amplitude of the vertical profile of aerosol mass is uniformly increased. Given NAAPS' goal of forecasting large visibility-reducing events, under most circumstances this simple method is sufficient. Again, with only 2-D satellite AOD observations available, this simple scaling technique is a valid first guess to redistribute column integrated AOD vertically.

[34] Difficulties arise if the NAAPS aerosol source function or transport meteorology totally misses an event that is observed in MODIS. Newly introduced aerosol features could be totally different from the model predictions in terms of aerosol species and vertical distributions. One of the solutions for this problem is to adopt a background bias correction technique [e.g., *Dee and da Silva*, 1998], which is the subject of ongoing research. As the first step of this study, two procedures are used to compensate for the problem: (1) for $\tau_{b\lambda} \geq 0.10$, the ratio of $(\tau_{b\lambda} + \hat{\tau}_\lambda)/\tau_{b\lambda}$ is still used to scale up the mass concentration of a given air column; (2) for $\tau_{b\lambda} < 0.10$, a seasonal 3-D aerosol climatology created using 3 years (2004–2006) of NAAPS data is used. The NAAPS 3-D aerosol climatology was constructed for dust, smoke, and sulfate aerosols, for broad regions (60° longitude by 30° latitude).

4.4. Forecast

[35] As shown in Figure 1, we separated NAAPS model runs into two modes: assimilation run mode and forecast run mode. The assimilation run mode is defined as the NAAPS run initialized with NAVDAS-AOD analyses every 6 h interval. The free-running forecast or nonassimilation run mode refers to the time step when NAAPS model runs in a forecast mode without invoking the NAVDAS-AOD procedures described in sections 4.1–4.3. Since forecast accuracy is more important for operational models, in this study, we evaluated the impact of aerosol data assimilation not only to NAAPS assimilation runs, but also to NAAPS forecasts.

5. Derivation of the Error and Error Covariance Matrices

[36] As discussed in section 4, both background (model space) and observational error covariance matrices are critical to the aerosol data assimilation process and are tightly connected through the physics of measurement. The error covariance matrices are composed of diagonal terms and nondiagonal terms. The diagonal terms represent error variances, and the nondiagonal terms represent spatial error covariances. In the following section, we show our estimates of both diagonal and nondiagonal terms of the observational error covariance matrix in section 5.1 and show the NAAPS model error covariance matrix in section 5.2.

5.1. Observational Coverage and Errors

[37] In this study, we assume that observational errors are uncorrelated. That is, the error in one 1° × 1° MODIS level 3 aggregate is uncorrelated to the ones adjacent to it. In reality, this is certainly not the case. Because the MODIS algorithm is sensitive to aerosol microphysics (e.g., smoke versus dust) and the lower boundary condition (glint, whitecapping), any large aerosol feature will have correlated errors. However, in the QA and correction procedures of *Zhang and Reid* [2006], most of the systematic uncertainties have been corrected. While this data treatment is by no means perfect, it does reduce correlated errors.

[38] The reason why this assumption is important is that it will zero out all the nondiagonal elements of the observational error covariance matrix, which leaves only diagonal elements as the nonzero terms. The diagonal elements are simply observational error variances and are estimated using both instrumental error variance (σ_i^2) and sample error variance (σ_s^2) or so-called spatial representative error variance. To estimate σ_i^2, we used the RMS instrument error variance as suggested by *Zhang and Reid* [2006], which is similar after corrections to that proposed by *Remer et al.* [2005] for $\tau < 0.6$. The σ_s^2 represents spatial data variation and is estimated by the spatial sample variance from the averaging of MODIS τ at $1^\circ \times 1^\circ$ area. The total observational error variance (σ_o^2) is simply defined as equation (5):

$$\sigma_o^2 = \sigma_s^2/n + \sigma_i^2 \tag{5}$$

[39] In contrast with some of the studies that estimate background and observational error variances and/or disentangle the individual components of the observation errors using innovation statistics [e.g., *Dee and da Silva*, 1998, 1999], we used AERONET optical depth observations that are independent from both model and satellite observations. The drawback of this approach is that AERONET observations are point source observations and may not represent the bin-averaged AOD values in some cases. However, AERONET data, which is not included in the assimilation process, provide independent evaluations of both background and satellite error variances.

5.2. Background Error and Error Covariance Matrix

[40] The model background error covariance matrix is critical to the aerosol data assimilation as it determines the impact ranges of observations. For any given two grid locations, m and n, where for the 1° NAAPS model m and n ranging from 1 to 360×180, the background error covariance between the two grid points (P_b^{mn}) can be estimated as:

$$P_b^{mn} = \left[S_b^m\right]^{1/2} C_b^{1/2} \left[S_b^n\right]^{1/2}, \tag{6}$$

where S_b^m and S_b^n are error variances at location m and n, respectively (also the diagonal terms of the error covariance matrix), and C_b is the error correlation between point m and n. The NAAPS error variance (S_b) is estimated as a function of NAAPS τ, based on half year (January–June 2006) of analysis using NAAPS and AERONET data. To estimate S_b, we first computed model error variances for every 0.1 NAAPS τ interval (for $\tau < 1.0$) and then applied a linear regression through these error variance values. The overall square root of NAAPS model error variance is estimated to be $0.20 + 0.4\tau$ for NAAPS nonassimilation runs and is $0.15 + 0.3\tau$ for NAAPS 6 h forecast with assimilation.

[41] Give the fact that C_b contains $64{,}800 \times 64{,}800$ array elements and is computationally expensive to estimate each single term, we estimated C_b using the second order autoregressive (SOAR) function [*Daley and Barker*, 2001], as the horizontal correlation model and is shown in equation (7):

$$C_b(m,n) = (1 + R_{mn}/L)exp(-R_{mn}/L) \tag{7}$$

where R_{mn} is the great circle distance and L is the global averaged horizontal error correlation length. A value for L of 200 km is used in this study. We validated our choice of L in section 6.3 by studying the spatial correlation of observation minus forecast.

6. Results from NAVDAS-AOD

[42] Using the new over-water level 3 MODIS product [*Zhang and Reid*, 2006] from January to May 2006, we evaluated the performance of the NRL aerosol data assimilation package. In section 6.1, we show a case study over the west coast of Africa; in section 6.2, we assess the impact of aerosol assimilation on NAAPS performance globally with the use of AERONET and MODIS data.

6.1. An African Case Study

[43] To demonstrate the impact of data assimilation on NAAPS fields, we use African dust as an example. Figure 2a shows the Terra MODIS true color image over the west coast of Africa for 30 May 2006. A large dust outbreak is observed off the coast of North Africa. Figure 2b shows the daily 1° (latitude/longitude) averaged τ from the combined (Terra+ Aqua) data assimilation quality level 3 MODIS aerosol product. Consistent with Figure 2a, heavy dust plumes with τ around 0.5 appear over the west coast of North Africa. Note that as mentioned in section 2, stringent data screening methods were applied to the operational level 2 MODIS aerosol product during the process of constructing a daily gridded MODIS aerosol product that meets the data assimilation standard. Therefore, we expect a much reduced spatial coverage from the newly developed MODIS level 3 aerosol product, compared with the operational level 2 MODIS aerosol product. Figure 2c shows the τ plot from the NAAPS nonassimilation run (without use of NAVDAS-AOD) for 1200 UTC, 30 May 2006. The NAAPS nonassimilation run underestimated both the strength and spatial coverage of the heavy dust plumes shown in Figures 2a and 2b. Figure 2d shows the result after continuous NAAPS assimilation runs from 1 January 2006. As illustrated in Figure 2d, the NAAPS model run with the NAVDAS-AOD included, captures both high τ regions over the coast regions and the transport path of the dust plumes across the Atlantic Ocean.

6.2. Global Statistics

[44] To evaluate the impact of the data assimilation process on NAAPS globally, we compared results to AERONET data [*Holben et al.*, 1998]. Since only over-ocean MODIS aerosol retrievals were used in this study, our comparisons were limited to the coastal and island AERONET sites. Note that AERONET data are point source data and may not necessarily represent $1^\circ \times 1^\circ$ bin averaged mean AOD values. A total of 5 months of AERONET optical depth data from January to May 2006 were included, and one pair of NAAPS and AERONET data were selected for in the analysis when the time gap between the NAAPS and AERONET data was within ±30 min.

[45] Figure 3a shows the scatterplot of NAAPS nonassimilation run and Sun photometer τ. The overall correlation between the two variables is 0.49. The absolute errors, estimated using all data points and separately using

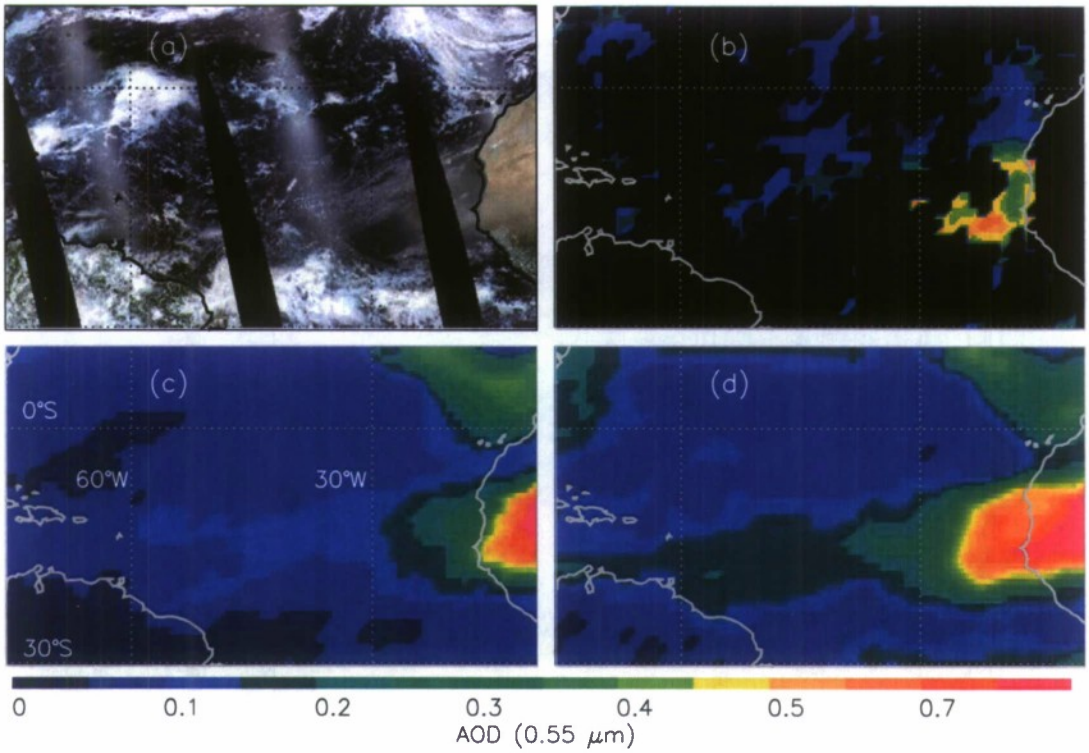

Figure 2. (a) MODIS true color image for 30 May 2006; (b) daily averaged MODIS (Terra + Aqua) τ for the same day as Figure 2a. Notice that with the stringent data cleaning processes, Figure 2b may be different from the plot that is created using the operational level 2 MODIS aerosol product; (c) NAAPS τ analysis for 1200 z, 30 May 2006, without the use of NAVDAS-AOD; (d) NAAPS τ analysis for 1200 z, 30 May 2006, with 5 months of data assimilation.

data points that have AERONET τ larger than 0.2 are 0.11 and 0.23, respectively. However, these statistics are misleading in that a multimodal data distribution pattern is observed. The vertical population (Sun photometer $\tau < 0.5$, NAAPS $\tau \gg 0.5$) represents events that are overpredicted by NAAPS. The horizontal population (NAAPS $\tau < 0.5$, Sun photometer $\tau \gg 0.5$) represents events that are missed or underpredicted by NAAPS. Both errors may also be due to an aerosol event in NAAPS that is phase-shifted from its real location. This is particularly likely near and downwind of underreported regions of the world such as Africa and South America.

[46] Nevertheless, once data assimilation is included, we find a remarkable improvement. Figure 3b shows the scatterplot of AERONET versus NAAPS τ for the NAAPS data from the NAVDAS-AOD mode runs. With the inclusion of MODIS data, the correlation between NAAPS and AERONET τ is improved to 0.73, and more importantly we found a 40% reduction in absolute errors for all data points and for data points with AERONET τ larger than 0.2.

[47] To increase spatial coverage over the ocean, we also compared NAAPS data against the level 3 MODIS data that were developed by *Zhang and Reid* [2006]. As an example, Figure 4a shows the scatterplot of over-ocean MODIS τ versus NAAPS τ (from nonassimilation run) for the period of March to May 2006 were used (the NAAPS and MODIS data from the full range of the study period is not shown, as the data volume is enormous and similar plots like Figure 4 were found for every single month). As with AERONET comparison, a multimodal pattern is also observed in comparing with daily gridded MODIS data (Figure 4a). This is due to the reasons described in the previous paragraph, indicating a need for improving NAAPS forecast accuracy through various means, including the use of the NAVDAS-AOD. Figure 4b shows the scatterplot of MODIS τ versus NAAPS τ (with the NAVDAS-AOD included) for the same time period as Figure 4a. Since MODIS data were used in the NAAPS assimilation mode runs, therefore, instead of comparing MODIS data with the NAAPS data from the assimilation mode runs, we compared MODIS data with the NAAPS data from the 6 h forecast mode runs. The NAVDAS-AOD is used to modify the NAAPS initial condition at t = 0, using MODIS data from -3 h $<$ t $<$ +3 h. NAAPS is then run in forecast mode to t = +6 h, and the result are compared with MODIS observations having +3 h $<$ t $<$ +9 h. With the use of the NAVDAS-AOD, even after 6 h forecast run, the correlation is improved from 0.57 to 0.81, and the absolute error reduced by 40–50% for all data points and for data points with AERONET $\tau > 0.2$ as well. Figure 3 and 4 indicate that with careful QA and QC processes, satellite data can benefit aerosol forecasts.

[48] Figure 4 demonstrates the influence of aerosol data assimilation through point comparisons between MODIS and NAAPS τ. Figure 5 further illustrates the regional differences in NAAPS model runs with and without the inclusion of the NAVDAS-AOD. Figure 5a shows the

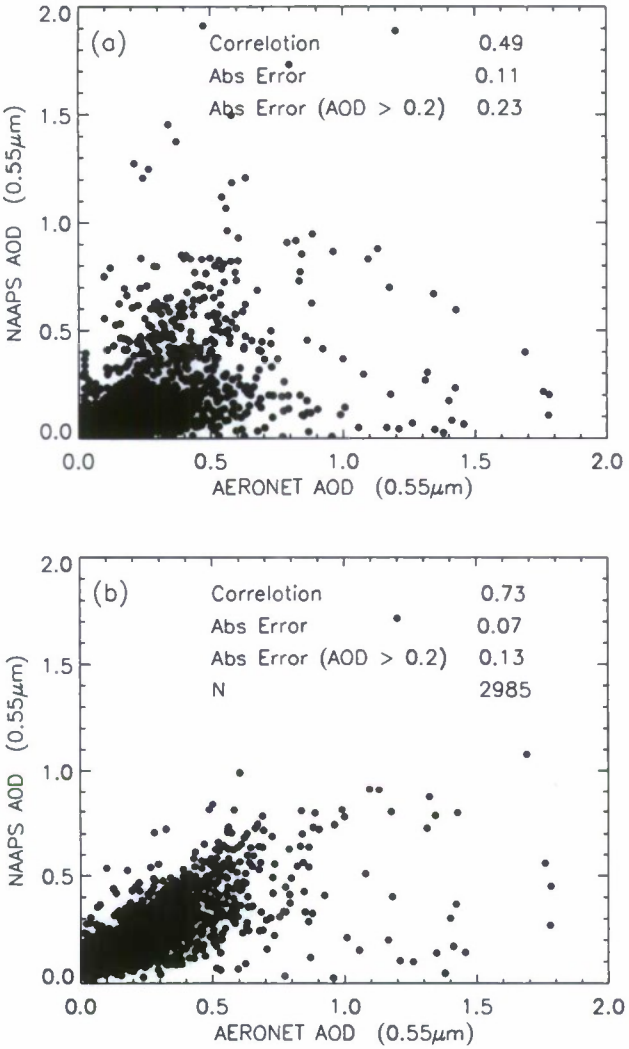

Figure 3. (a) AERONET versus NAAPS τ for 5-month (January–May 2006) NAAPS nonassimilation run; (b) AERONET versus NAAPS τ for 5-month (January–May 2006) NAAPS run with the aerosol data assimilation process.

3 month averaged (March–May 2006), 1° × 1° latitude/longitude gridded MODIS τ from the MODIS level 3 products used in this study. Outliers are more damaging to NAVDAS-AOD analysis quality than data losses. Therefore, in the newly developed MODIS level 3 aerosol products, stringent data screening processes (as explained in section 2) were applied to reduce noise and outliers. Hence, the 3 month averaged MODIS τ plot showed in Figure 5a could be different from the plot generated using the operational MODIS level 2 product. For example, there are data gaps (in black) over the high-latitude southern hemisphere, due to high frequency of cloud cover over that region, which may not be observed if the plot is generated using operational MODIS level 2 aerosol product. In Figure 5a, large dust aerosol fronts are visible off the West Coast of Africa and East Coast of Asia. Biomass burning smoke is observed over Central America and the northwest coast of North America, and pollutant aerosols are found over India.

Figure 5b shows the averaged NAAPS τ from NAAPS nonassimilation runs for the same period as Figure 5a. The NAAPS nonassimilation runs could reproduce dust aerosol fronts shown in Figure 5a. However, the magnitudes of the dust optical depth are underestimated for both regions. Furthermore, the NAAPS nonassimilation runs miss the major biomass burning and the pollutant aerosol plums that are visible in Figure 5a. Figure 5c shows the three month averaged NAAPS τ from the assimilation runs. The NAAPS assimilation runs successfully reproduce both the spatial distributions and magnitudes of the dust episode and are also able to simulate the smoke and pollutant aerosol plumes missed by the NAAPS nonassimilation runs.

[49] We also evaluated the performance of NAAPS 6-h forecasts. Figure 5d shows the 3-month averaged NAAPS 6-h forecast runs after ingesting observations at the analysis time t = 0. Similar patterns of τ are shown as

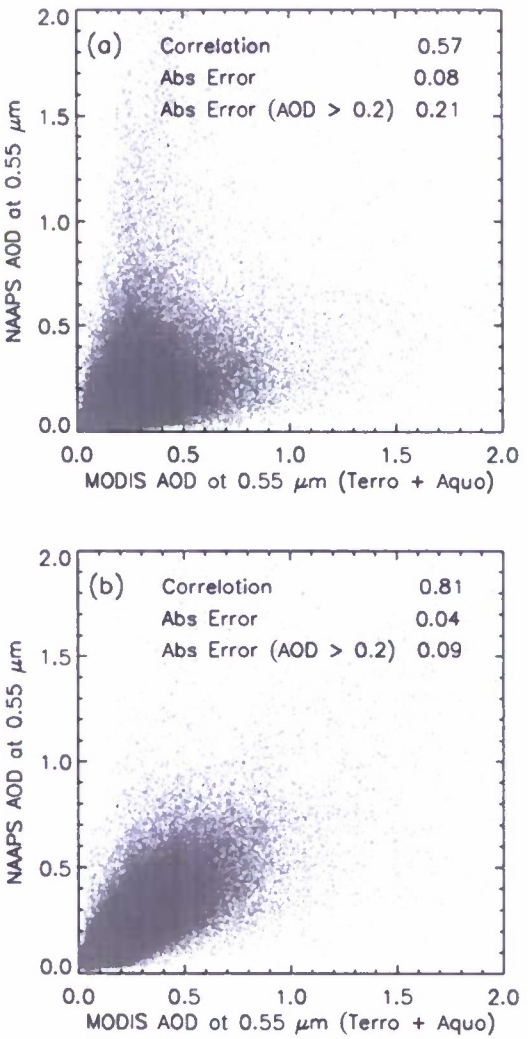

Figure 4. (a) MODIS versus NAAPS τ for 3-month (March–May 2006) NAAPS nonassimilation run; (b) MODIS versus NAAPS τ for 3-month (March–May 2006) NAAPS 6-h forecast run (t = +6 h). The NAVDAS-AOD is used to modify the NAAPS initial condition at t = 0.

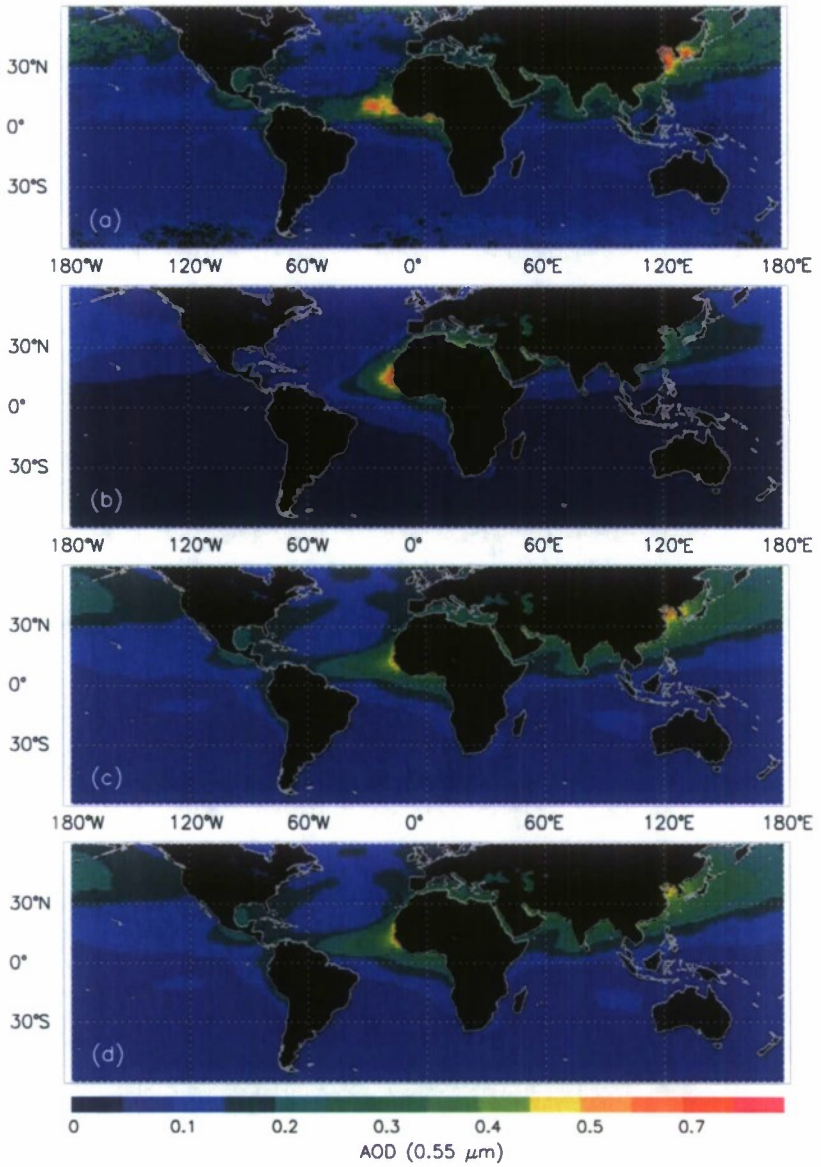

Figure 5. (a) Three-month (March–May 2006) averaged MODIS (Terra + Aqua) τ. Notice the newly developed MODIS level 3 product is used. Therefore, there could be discrepancies between Figure 5a and the image that is created using the operational MODIS level 2 aerosol product (see section 6.2); (b) 3-month (same months as Figure 5a) averaged NAAPS τ (total) from NAAPS nonassimilation run; (c) 3-month (same months as Figure 5a) averaged NAAPS τ (total) from NAAPS assimilation run. (d) Three-month (same months as Figure 5a) averaged NAAPS τ (total) from 6-h NAAPS forecast run after assimilation run at t = 0.

Figure 5c with slight reductions in magnitude, indicating that the NAVDAS-AOD improves model performance at even the 6-h forecast timescale. The globally averaged τ over oceans are approximately 0.13, 0.06, 0.12, and 0.12 for Figures 5a–5d, respectively. NAAPS nonassimilation runs underestimate the magnitude of globally averaged τ over oceans, while with the use of NAVDAS-AOD, NAAPS aerosol forecasting performance is improved.

[50] As NAAPS is an operational aerosol forecasting model, we are not only interested in the improvement in NAAPS' aerosol analysis when satellite data are available but are also interested in whether the use of NAVDAS-AOD at time t = 0 could help aerosol forecasts for a longer period. Figure 6a shows the absolute error ($|\Delta\tau|$, in absolute difference) between NAAPS and AERONET τ values (coast and island sites) as a function of forecast hour in the forecast mode run. Data from March to May of 2006 were used in the analysis. The dashed lines show the $|\Delta\tau|$ values for NAAPS nonassimilation run. The solid lines show the $|\Delta\tau|$ values when the NAAPS run in the assimilation mode before and at forecast time 0 but not in any other time after forecast time 0. The black line with diamond symbols shows the $|\Delta\tau|$ values for all data points

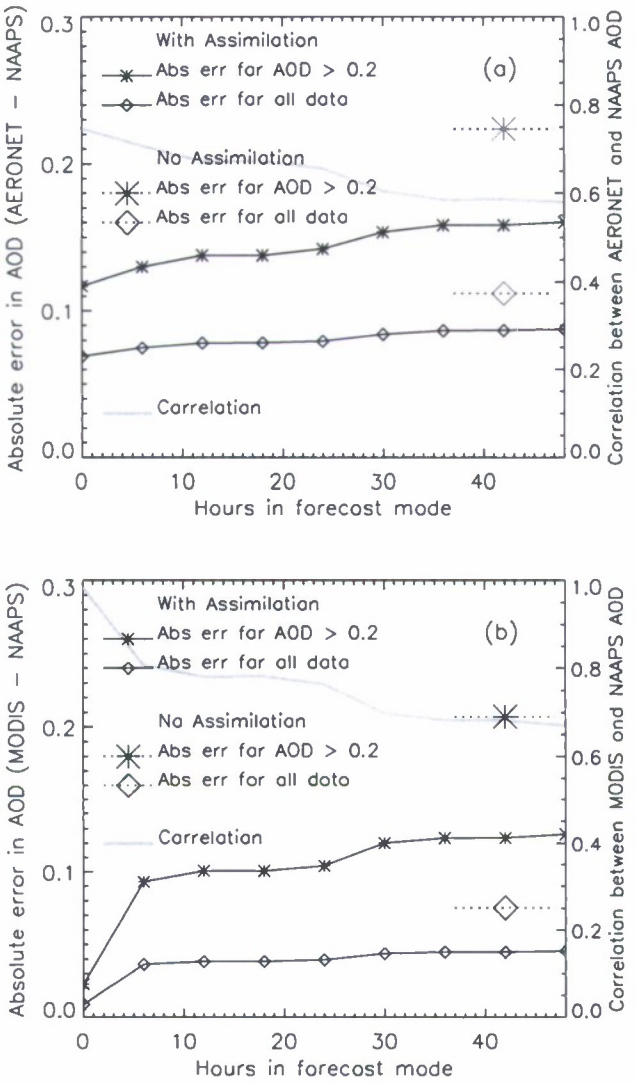

Figure 6. (a) Three-month (March–May 2006) averaged differences between AERONET and NAAPS (nonassimilation run) τ as a function of number of hour in forecast mode run. The black line with diamond symbols is derived using all data points. The black line with star symbols is derived using pairs of AERONET and NAAPS data with AERONET τ larger than 0.2. Light gray line shows correlation between AERONET and NAAPS τ as a function of forecasting time; (b) 3-month (March–May 2006) averaged differences between MODIS and NAAPS (with data assimilation at time 0) τ as a function of number of hour in forecast mode run. The definitions for solid block, and light gray lines are similar to that of Figure 6a, except for MODIS and NAAPS analyses.

and the black line with star symbols shows the $|\Delta\tau|$ values for data points with Sun photometer τ larger than 0.2.

[51] When all data were used in the analysis, the absolute difference between AERONET and NAAPS τ with the use of NAVDAS-AOD is 0.07 at forecast time 0 (A 40% reduction in $|\Delta\tau|$). As expected, $|\Delta\tau|$ values increase with time during the forecast run. However, even after 48 h of forecast run, the absolute error is about 20% less than that without the use of NAVDAS-AOD. The improvements hold for larger aerosol events. For example, the black line with star symbols shows the same analysis as the black line with diamond symbols for data points with AERONET τ larger than 0.2, with a reduction in error of about 20%. The light gray line in Figure 6a shows the correlation between AERONET and NAAPS τ as a function of NAAPS forecasting time. After 48 h of NAAPS run in a nonassimilation mode, the correlation is reduced from 0.75 to 0.58.

[52] We repeated the analysis using MODIS over-ocean data (Figure 6b). The low $|\Delta\tau|$ values at time 0 (solid black lines) are due to MODIS data ingested in the assimilation process at time 0. For up to 48 h in forecast mode run, the $|\Delta\tau|$ values for all data points and for data points with AERONET $\tau > 0.2$ are 30–40% lower than the $|\Delta\tau|$ values estimated using the NAAPS data from the nonassimilation run. Note that in Figure 6b, from t = 0 h to t = 6 h, there is a sudden increase in absolute error. The sudden increase in absolute error could be attributed to the fact that over ocean satellite data are ingested at t = 0 h, while at t = 6 h, large

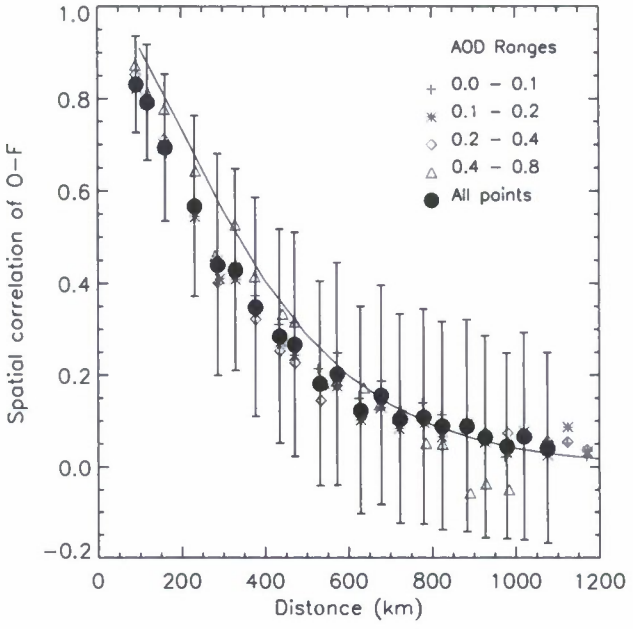

Figure 7. Spatial correlations of satellite observation (O) minus NAAPS 6-h forecast (F) as a function of distance. Averaged (every 50 km) spatial correlations of O-F are shown for four different MODIS τ ranges: 0.0–0.1 (plus sign), 0.1–0.2 (star), 0.2–0.4 (diamond), and 0.4–0.8 (triangle), and for all MODIS τ ranges (solid black dots). Vertical bars show one standard deviation of the averaged spatial correlation for all MODIS τ ranges. Black line shows the SOAR function (equation (7)) fit with L set to 200 km.

forecasting errors are propagated from inland continents to global oceans along the costal lines. Similar to Figure 6a, the gray line shows the correlation between MODIS and NAAPS τ as a function of forecasting time. Again, as expected, the correlation reduces as forecasting time increases. Although, even after 48 h the forecast is substantially better with data assimilation. It worth mentioning that at time 0, the correlation between MODIS and NAAPS τ is near 1, which indicates that NAVDAS-AOD package properly merges MODIS aerosol optical depth data into the analysis fields.

6.3. Innovation Checks and Problems

[53] In this section, we evaluated the differences between satellite observation (O), and 6 h mode forecast (F, at t = 6 h). Figure 7 shows the spatial correlation of O minus F (O-F) as a function of distance. The spatial correlation of O-F for two given locations (m,n) is used to represent $C_b(m, n)$ in equation (7). Both satellite and forecasting data from March to May 2006 were used. To calculate spatial correlation of O-F for two given locations, we require that there are at least 30 pairs of O-F values with identical time tags, and we assume a zero spatial correlation for any two locations separated by more than 2000 km. Figure 7 shows the spatial correlation of O-F as a function of distance for four MODIS τ ranges: 0.0–0.1 (plus sign), 0.1–0.2 (star), 0.2–0.4 (diamond), and 0.4–0.8 (triangle), and for all MODIS τ ranges (solid black dots). The vertical bars represent one standard deviation to the spatial correlation values for all MODIS τ ranges. The black line, which is calculated using equation 7 with L set to 200 km, fits well with the solid black dots. This indicates that L value of 200 km is a reasonable estimation of the background error correlation length.

[54] We also examined the spatial distributions of O-F, and O minus analysis (A, at t = 0 h). Figure 8a shows the map of 3-month averaged O-A, and Figure 8b shows the square root of variance (STD) of O-A for March–May 2006. Since a high correlation of above 0.98 is constantly observed between O and A, it is not surprised to see that the 3 month mean and STD of O-A values are near-zero spatially.

[55] Figure 8c and 8d show the 3 month averaged O-F, and the square root of variance of O-F, respectively, for the same study period as Figure 8a and 8b. In Figure 8c and 8d, the global averaged O-F value is less than 0.01 and the global averaged STD value is on the order of 0.05. However, large O-F values are observed over west coast of Africa where consistent dust plumes are located. High O-F values are also found over east Asia. Given the fact that only over-ocean MODIS data were used in the assimilation process, the high O-F values are mostly introduced by propagating of forecast errors from land to ocean. However, the large O-F values may also be due to the following factors:

[56] 1. Background error correlation is assumed to be isotropic in this study. However, this is not a good assumption for regions with sharp aerosol fronts.

[57] 2. Existence of forecast biases. A background bias correction scheme [e.g., *Dee and da Silva*, 1998; 1999], as a function of region and season, may need to be implemented in a future version of NAVDAS-AOD.

7. Discussion, Conclusion, and Future Work

[58] In this paper, we present a new aerosol data assimilation package that is currently running in a pseudo-operational mode with the Naval Research Laboratory, Marine Meteorology Division's NAAPS model. A 2-D

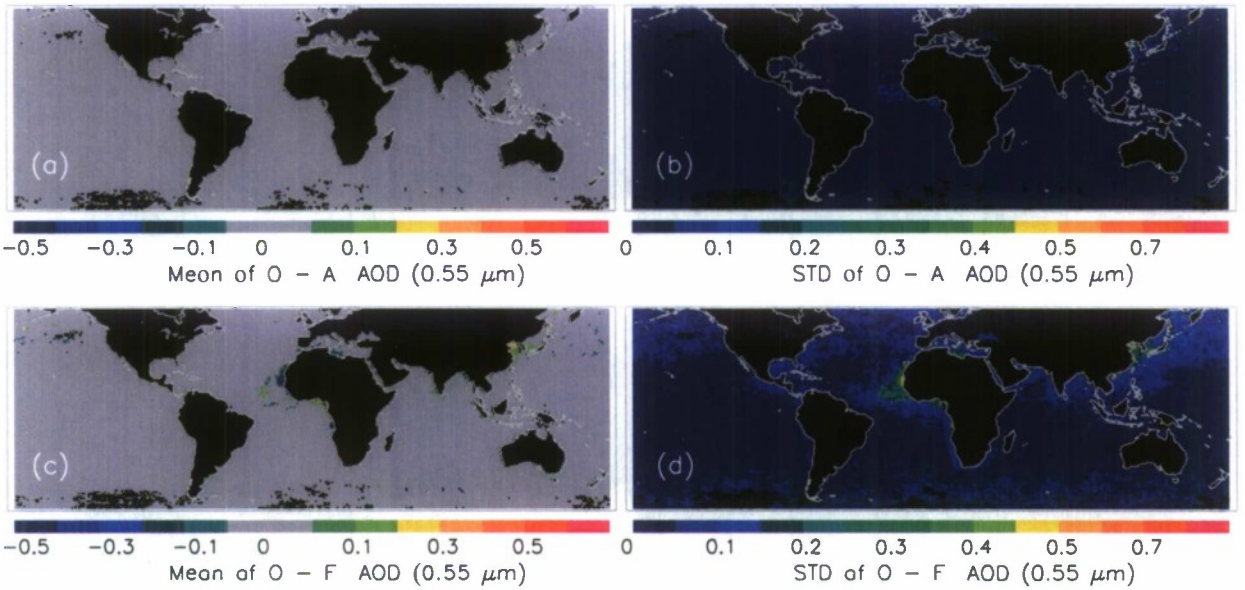

Figure 8. (a) Global map of the three month averaged satellite observation (O) minus NAAPS analysis (A) values for March–May 2006. (b) Square root of variance (STD) of O-A. (c) Similar to Figure 8a but for O-F. (d) Similar to Figure 8b but for O-F.

variational technique based on NAVDAS is used to integrate model output from NAAPS and satellite observations from a newly developed MODIS level 3 product. The new level 3 MODIS aerosol product is generated from the operational MODIS aerosol level 2 product through rigorous QA processes. An overall assessment of the NAVDAS-AOD and directions for future research are listed as follows:

[59] 1. With the use of satellite observations from MODIS, especially with careful data screening process, our study indicates that the NAVDAS-AOD not only improves the accuracy of analyzed global aerosol distribution at times when satellite data are available, but also improves the accuracy of the estimations in a forecast mode for 48 h or more.

[60] 2. One major problem with this study is the three-dimensional redistribution of aerosol plumes when NAAPS reports an erroneously low τ value. This happens when NAAPS misses an aerosol feature. To address this problem, 3-D observations from CALIPSO system are needed for future evaluation.

[61] 3. As suggested in section 6.3, a background bias correction method [e.g., *Dee and da Silva*, 1998; 1999] needs to be explored and possibly used in a future version of NAVDAS-AOD.

[62] 4. This study focused on over-ocean aerosol data assimilation. An over-land aerosol data assimilation process is being developed in a separate project.

[63] 5. The error covariance matrix for both background and observations are critical for the data assimilation process. In this study, the errors in observations are assumed to be uncorrelated. The nondiagonal terms of background error covariance matrix are estimated using a SOAR function with a specified error correlation length estimated from the differences between MODIS and NAAPS τ. However, as illustrated in the paper, the error correlation length varies as a function of location and time and is most significant when large acrosol plumes exist. In future studies, we plan to implement a regional error correlation length model and, eventually, a simplified version of the real error correlation matrix as computations permit.

[64] 6. The NAVDAS-AOD is currently running quasi-operationally and the NAAPS data with the assimilation can be accessed through www.nrlmry.navy.mil/aerosol/ in the near future.

[65] **Acknowledgments.** This manuscript required the use of many coastal and island AERONET sites. We are most grateful to the international federated AERONET program and Brent Holben (NASA GSFC) in particular for the data they provide. We also thank Clay Blankenship and Bill Campbell for their tremendous help and suggestions. This research was funded by the Office of Naval Research Code 322 (N0001405WR20206) and the Joint Center for Satellite Data Assimilation. Jianglong Zhang is a UCAR visiting scientist.

References

Baker, N. L., T. F. Hogan, W. F. Campbell, R. L. Pauley, S. D. Swadley (2005), The impact of AMSU-A radiance assimilation in the U. S. Navy's Operational Global Atmospheric Prediction System (NOGAPS), *Memo. Rep. NRL/MR/7530–05–8836*, Naval Res. Lab., Monterey, Calif.

Benkovitz, C. M., M. T. Scholtz, J. Pacyna, L. Tarrason, J. Dignon, E. C. Voldner, P. A. Spiro, J. A. Logan, and T. E. Graedel (1996), Global gridded inventories of anthropogenic emissions of sulfur and nitrogen, *J. Geophys. Res.*, *101*(D22), 29,239–29,253, doi:10.1029/96JD00126.

Christensen, J. H. (1997), The Danish Eulerian hemispheric model - A three-dimensional air pollution model used for the Arctic, *Atmos. Environ.*, *31*(24), 4169–4191, doi:10.1016/S1352-2310(97)00264-1.

Collins, W. D., P. J. Rasch, B. E. Eaton, B. V. Khattatov, J.-F. Lamarque, and C. S. Zender (2001), Simulating aerosols using a chemical transport model with assimilation of satellite aerosol retrievals: Methodology for INDOEX, *J. Geophys. Res.*, *106*(D7), 7313–7336, doi:10.1029/2000JD900507.

Dabberdt, W. F., and T. W. Schlatter (1996), Research opportunities from emerging atmospheric observing and modeling capabilities, *Bull. Am. Meteorol. Soc.*, *77*, 305–323, doi:10.1175/1520-0477(1996)077<0305:ROFEAO>2.0.CO;2.

Daley, R., and E. Barker (2001), NAVDAS: Formulation and diagnostics, *Mon. Weather Rev.*, *129*(4), 869–883, doi:10.1175/1520-0493(2001)129<0869:NFAD>2.0.CO;2.

Dee, D., and A. da Silva (1998), Data assimilation in the presence of forecast bias, *Q. J. R. Meteorol. Soc.*, *124*, 269–295, doi:10.1002/qj.49712454512.

Dee, D., and A. da Silva (1999), Maximum-likelihood estimation of forecast and observation error covariance parameters. Part I: Methodology, *Mon. Weather Rev.*, *127*, 1822–1834, doi:10.1175/1520-0493(1999)127<1822:MLEOFA>2.0.CO;2.

Dee, D. P., L. Rukhovets, R. Todling, A. M. da Silva, and J. W. Larson (2001), An adaptive buddy check for observational quality control, *Q. J. R. Meteorol. Soc.*, *127*, 2451–2471, doi:10.1002/qj.49712757714.

Hanel, G. (1976), The properties of atmospheric aerosol particles as functions of relative humidity at thermodynamic equilibrium with surrounding moist air, *Adv. Geophys.*, *19*, 73–188.

Hegg, D. A., D. S. Covert, K. Crahan, and H. Jonsson (2002), The dependence of aerosol light-scattering on RH over the Pacific Ocean, *Geophys. Res. Lett.*, *29*(8), 1219, doi:10.1029/2001GL014495.

Hess, M., P. Koepke, and I. Schult (1998), Optical properties of aerosols and clouds: The software package OPAC, *Bull. Am. Meteorol. Soc.*, *79*(5), 831–844, doi:10.1175/1520-0477(1998)079<0831:OPOAAC>2.0.CO;2.

Hogan, T. F., and L. R. Brody (1993), Sensitivity studies of the Navy's global forecast model parameterizations and evaluation of improvements to NOGAPS, *Mon. Weather Rev.*, *121*(8), 2373–2395, doi:10.1175/1520-0493(1993)121<2373:SSOTNG>2.0.CO;2.

Hogan, T. F., and T. E. Rosmond (1991), The description of the Navy Operational Global Atmospheric Prediction Systems spectral forecast model, *Mon. Weather Rev.*, *119*(8), 1786–1815, doi:10.1175/1520-0493(1991)119<1786:TDOTNO>2.0.CO;2.

Holben, B. N., et al. (1998), AERONET - A federated instrument network and data archive for aerosol characterization, *Remote Sens. Environ.*, *66*, 1–16, doi:10.1016/S0034-4257(98)00031-5.

Hsu, N. C., S.-C. Tsay, M. D. King, and J. R. Herman (2006), Deep blue retrievals of Asian aerosol properties during ACE-Asia, *IEEE Trans. Geosci. Rem. Sens.*, *44*(11), 3180–3195, doi:10.1109/TGRS.2006.879540.

Husar, R. B., J. M. Prospero, and L. L. Stowe (1997), Characterization of tropospheric aerosols over the oceans with the NOAA advanced very high resolution radiometer optical thickens operational product, *J. Geophys. Res.*, *102*(D14), 16,889–16,909, doi:10.1029/96JD04009.

Kahn, R. A., B. J. Gaitley, J. V. Martonchik, D. J. Diner, K. A. Crean, and B. Holben (2005), Multiangle Imaging Spectroradiometer (MISR) global aerosol optical depth validation based on 2 years of coincident Aerosol Robotic Network (AERONET) observations, *J. Geophys. Res.*, *110*, D10S04, doi:10.1029/2004JD004706.

Kaufman, Y. J., D. Tanré, and O. Boucher (2002), A satellite view of aerosols in the climate system, *Nature*, *419*, 215–223, doi:10.1038/nature01091.

Levy, R. C., L. Remer, S. Mattoo, E. Vermote, and Y. J. Kaufman (2007), Second-generation algorithm for retrieving aerosol properties over land from MODIS spectral reflectance, *J. Geophys. Res.*, *112*, D13211, doi:10.1029/2006JD007811.

McNally, A. P., and M. Vesperini (1996), Variational analysis of humidity information from TOVS radiances, *Q. J. R. Meteorol. Soc.*, *122*, 1521–1544, doi:10.1002/qj.49712253504.

Ming, Y., and L. M. Russell (2001), Predicted hygroscopic growth of sea salt aerosol, *J. Geophys. Res.*, *106*(D22), 28,259–28,274, doi:10.1029/2001JD000454.

Rasch, P. J., W. D. Collins, and B. E. Eaton (2001), Understanding the Indian Ocean Experiment (INDOEX) aerosol distributions with an aerosol assimilation, *J. Geophys. Res.*, *106*(D7), 7337–7355, doi:10.1029/2000JD900508.

Reid, J. S., E. M. Prins, D. L. Westphal, C. C. Schmidt, K. A. Richardson, S. A. Christopher, T. F. Eck, E. A. Reid, C. A. Curtis, and J. P. Hoffman (2004), Real-time monitoring of South American smoke particle emissions and transport using a coupled remote sensing/box-model approach, *Geophys. Res. Lett.*, *31*, L06107, doi:10.1029/2003GL018845.

Reid, J. S., T. Eck, S. Christopher, O. Dubovik, R. Koppmann, D. Eleuterio, B. Holben, E. Reid, and J. Zhang (2005), A review of biomass burning emissions part III: Intensive optical properties of biomass burning particles, *Atmos. Chem. Phys.*, *5*, 827–849, SRef-ID:1680–7324/acp/2005–5-827.

Remer, L. A., et al. (2005), The MODIS aerosol algorithm, products and validation, *J. Atmos. Sci.*, *62*, 947–973, doi:10.1175/JAS3385.1.

Ritchie, H. (1987), Semi-Lagrangian advection on a gaussian grid, *Mon. Weather Rev.*, *115*(2), 608–619, doi:10.1175/1520-0493(1987)115<0608:SLAOAG>2.0.CO;2.

Slinn, S. A., and W. G. N. Slinn (1980), Predictions for particle deposition on natural-waters, *Atmos. Environ.*, *14*(9), 1013–1016, doi:10.1016/0004-6981(80)90032-3.

Staniforth, A., and J. Cote (1991), Semi-Lagrangian integrations schemes for atmospheric models-A review, *Mon. Weather Rev.*, *119*(9), 2206–2223, doi:10.1175/1520-0493(1991)119<2206:SLISFA>2.0.CO;2.

Tomassini, M., G. Kelly, and R. Saunders (1999), Use and impact of satellite atmospheric motion winds on ECMWF analyses and forecasts, *Mon. Weather Rev.*, *127*, 971–986, doi:10.1175/1520-0493(1999)127<0971:UAIOSA>2.0.CO;2.

Voldner, E. C., L. A. Barries, and A. Siroi (1986), A literature review of dry deposition of oxides of sulfur and nitrogen with an emphasis on long-range transport modeling in North America, *Atmos. Environ.*, *20*(11), 2101–2123, doi:10.1016/0004-6981(86)90305-7.

Walcek, C. J., R. A. Brost, J. S. Chang, and M. L. Wesely (1986), SO_2, sulfate and HNO3 deposition velocities computed using regional land-use and meteorological data, *Atmos. Environ.*, *20*(5), 949–964, doi:10.1016/0004-6981(86)90279-9.

Weaver, C., A. da Silva, M. Chin, P. Ginoux, O. Dubovik, D. Flittner, A. Zia, L. Remer, B. Holben, and W. Gregg (2007), Direct insertion of MODIS radiances in a global aerosol transport model, *J. Atmos. Sci.*, *64*, 808–826, doi:10.1175/JAS3838.1.

Westphal, D. L., O. B. Toon, and T. N. Carlson (1988), A case study of mobilization and transport of Saharan dust, *J. Atmos. Sci.*, *45*, 2145–2175, doi:10.1175/1520-0469(1988)045<2145:ACSOMA>2.0.CO;2.

Witek, M. L., P. J. Flatau, P. K. Quinn, and D. L. Westphal (2007), Global sea-salt modeling: Results and validation against multicampaign shipboard measurements, *J. Geophys. Res.*, *112*, D08215, doi:10.1029/2006JD007779.

Yu, H., R. E. Dickinson, M. Chin, Y. J. Kaufman, M. Zhou, L. Zhou, Y. Tian, O. Dubovik, and B. N. Holben (2004), Direct radiative effect of aerosols as determined from a combination of MODIS retrievals and GOCART simulations, *J. Geophys. Res.*, *109*, D03206, doi:10.1029/2003JD003914.

Zhang, J., and J. S. Reid (2006), MODIS aerosol product analysis for data assimilation: Assessment of level 2 aerosol optical thickness retrievals, *J. Geophys. Res.*, *111*, D22207, doi:10.1029/2005JD006898.

Zhang, J., J. S. Reid, and B. N. Holben (2005), An analysis of potential cloud artifacts in MODIS over ocean aerosol optical thickness products, *Geophys. Res. Lett.*, *32*, L15803, doi:10.1029/2005GL023254.

N. L. Baker, E. J. Hyer, J. S. Reid, and D. L. Westphal, Marine Meteorology Division, Naval Research Laboratory, 542 Sloat Avenue, Monterey, CA 93940, USA.

J. Zhang, Department of Atmospheric Sciences, University of North Dakota, 4149 University Avenue, Stop 9006, Grand Forks, ND 58202, USA. (jzhang@atmos.und.edu)